First light on an adaptive optics system using a non-modulation pyramid wavefront sensor for a 1.8 m telescope

Shengqian Wang (王胜千)[1,2,], Kai Wei (魏 凯)[1,2], Wenjia Zheng (郑文佳)[1,2], and Changhui Rao (饶长辉)[1,2,*]**

[1]*Key Laboratory on Adaptive Optics, Chinese Academy of Sciences, Chengdu 610209, China*
[2]*Institute of Optics and Electronics, Chinese Academy of Sciences, Chengdu 610209, China*
**Corresponding author: chrao@ioe.ac.cn; **corresponding author: wsq_ioe@126.com*
Received April 13, 2016; accepted August 19, 2016; posted online September 21, 2016

Our adaptive optics system based on a non-modulation pyramid wavefront sensor is integrated into a 1.8 m astronomical telescope installed at the Yunnan Observatory in LiJiang, and the first light with high-resolution imaging of an astronomical star is successfully achieved. In this Letter, the structure and performance of this system are introduced briefly, and then the observation results of star imaging are reported to show that the angular resolution of an adaptive optics system using a non-modulation pyramid wavefront sensor can approach the diffraction limit quality of a 1.8 m telescope.

OCIS codes: 010.1080, 010.7350.
doi: 10.3788/COL201614.100101.

Optical images of astronomical objects viewed through ground-based telescopes are blurred by the atmosphere[1]. Adaptive optics (AO) attempts to correct, in real time, the distortion induced by the turbulence in the incoming wavefront from the astronomical object of interest, thereby enabling the telescope to reach a diffraction-limited image quality[2]. The AO system uses a wavefront sensor to make measurements of the perturbations introduced by the atmosphere[3], so the wavefront sensor is a key element of the AO system, and its performance has a large influence on the effectiveness of wavefront correction of the AO system[4]. The pyramid wavefront sensor (PWFS) was first proposed by Ragazzoni in 1996 for astronomical AO[5], and it has been widely investigated for applications due to its superiority in adjustable gain and flexible sampling sub-apertures, which makes the PWFS increase the number of accessible scientific targets by more efficiently using guiding star photons. Thus, the PWFS is an attractive option for the next large telescope AO system compared with the Shack–Hartmann wavefront sensor[6,7]. The PWFS has been successfully used in the Telescopio Nazionale Galileo telescope and the Large Binocular Telescope, and encouraging on-sky results have been achieved[8,9]. This sensor is also investigated for implementation on the giant Magellan telescope and the Very Large Telescope Optics Facility[10,11]. At present, there are no relevant reports of the PWFS being used in large telescopes in China. In 2014, the PWFS was successfully applied to the 1.8 m telescope at the Yunnan Observatory, and first light on the AO system based on this sensor is reported in this Letter.

The 1.8 m telescope at the Yunnan Observatory is a Cassegrain optical structure, and light from a star is reflected by the primary mirror, the secondary mirror, the third mirror, and the other five reflective mirrors in the Coude room. The 127-element AO system installed on the 1.8 m telescope works based on the a Shack–Hartmann wavefront sensor with a 13×13 sub-aperture microlens array, and the first light on high-resolution imaging for stars was achieved in 2009[12].

In 2014, the new AO system, based on the PWFS and installed on the telescope, provided an alternate wavefront sensor for the existing AO system with a Shack–Hartmann wavefront sensor. The AO system based on the PWFS was installed in the Coude room (Fig. 1). First, the light rays originating from the natural star reach the Coude focal plane. After propagating through the reflective mirror M1 and the off-axis parabolic mirror PR1_1, the parallel light beam matching the pupil of the tracking system was obtained, and then, through a beam splitter BS1, the light was separated into the tracking system and the reflective mirror M2. The tracking system was used to provide the preliminary correction of the wavefront tilt, which ensures that the beam of light can enter the detection field of the PWFS. With the off-axis parabolic mirrors PR1_2 and PR1_3, the light beam reflected by BS1 was extended to match the pupil of the tilt mirror and the 127-element deformable mirror (DM). Finally, the beam was reduced using the off-axis parabolic mirrors PR2_1 and PR2_2 to match the pupil of the PWFS and the far-field imaging system. The transmission beam from the beam splitter BS2 enters the PWFS, and the reflective beam was transmitted into the far-field imaging system. The detector of the PWFS was an OCAM2 camera, and the corresponding frame rate of the PWFS is 1500 Hz. A Cascade camera was used as the far-field imaging detector, and the imaging band was 700 to 900 nm.

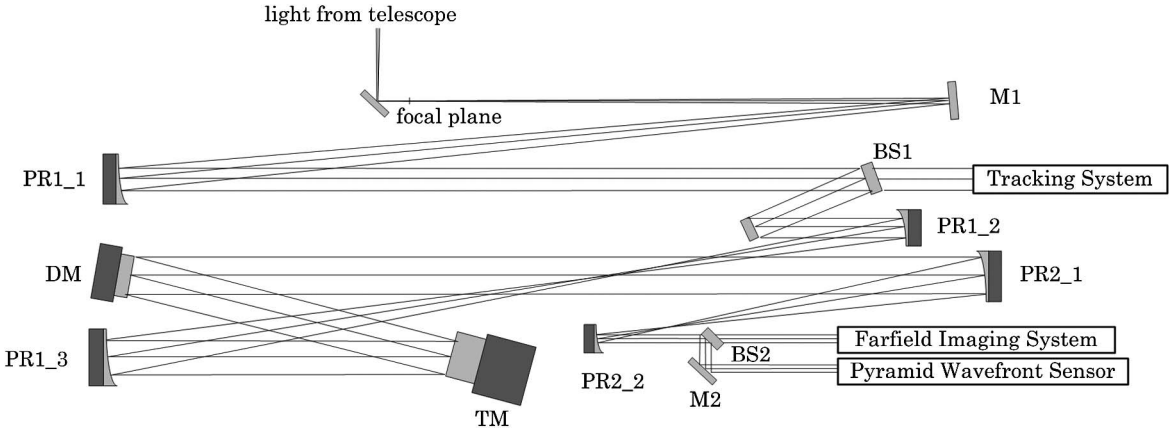

Fig. 1. Optical layout of the AO system based on the PWFS for 1.8 m telescope. M: reflective mirror, PR: parabolic mirror, TM: tilt mirror, BS: beam splitter mirror.

The spectral bandwidth of the imaging system is 700 to 900 nm, and the telescope diameter is 1760 mm. If the center wavelength 800 nm is used as the calculation parameter, the diffraction-limited angular resolution can be calculated according to the following formula:

$$\frac{\lambda}{D} = \frac{0.8\ \mu\text{m}}{1760\ \text{mm}} = 0.4546\ \text{urad} = 0.0938''. \tag{1}$$

The optical layout of the PWFS is illustrated in Fig. 2. The light rays through a focusing lens are focused on the top of a refractive pyramid with four sides, which splits the incoming beam into four separate beams, and then a relay lens re-images the four sub-pupils corresponding to each beam onto the detector camera. If the wavefront is not aberrated, the light is equally split by the refractive pyramid and the four sub-pupils are equally and uniformly illuminated. If wavefront is aberrated by turbulence, the intensity difference of these four sub-pupil images contains essential information about the optical aberrations.

The intensity distributions of these four sub-pupil images on the detector camera are expressed, respectively, as I_1, I_2, I_3, and I_4, and the detection signals of the PWFS in the x and y directions are calculated with the following formulas[5]:

$$S_x(x,y) = \frac{I_1(x,y) + I_4(x,y) - I_2(x,y) - I_3(x,y)}{I_1(x,y) + I_2(x,y) + I_3(x,y) + I_4(x,y)}, \tag{2}$$

$$S_y(x,y) = \frac{I_1(x,y) + I_2(x,y) - I_3(x,y) - I_4(x,y)}{I_1(x,y) + I_2(x,y) + I_3(x,y) + I_4(x,y)}. \tag{3}$$

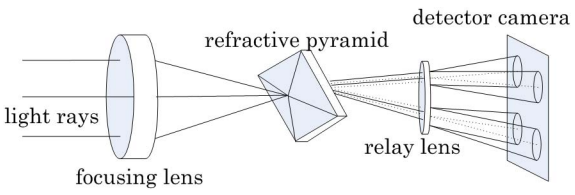

Fig. 2. Schematic diagram of the PWFS.

When the PWFS is used with modulation by oscillating the optical component, the linear measurement range is increased. Let us consider that the beam is modulated with a circular path with an angular amplitude θ. If the gradient of the aberration is smaller than the modulation θ in the linear measurement range, the PWFS signals relate to the wavefront slope by the formulas[13]

$$\frac{\partial W}{\partial x} \approx \theta \cdot S_x(x,y), \tag{4}$$

$$\frac{\partial W}{\partial y} \approx \theta \cdot S_y(x,y). \tag{5}$$

This linear modulation scheme is used for the calibration of the AO loop closing. In an astronomical AO system like the one presented here, atmospheric turbulence provides for the modulation of the beam around the PWFS[14]. The non-modulation mode is thus selected here to simplify the AO design. If no modulation is applied, the formula between the wavefront $\phi(x,y)$ and the PWFS signal $S_x(x,y)$ is given by the following expression (the same formula as the PWFS signal $S_y(x,y)$)[15]:

$$S_x(x,y) = \frac{1}{\pi}\int_{-B(y)}^{B(y)} p.v.\frac{\sin[\phi(x',y) - \phi(x,y)]}{x' - x}\,\mathrm{d}x'. \tag{6}$$

In Eq. (6), the parameter $B(y)$ is the x value of the pupil edge at y. Equation (6) shows that the PWFS signal is generated by the phase variations on the entire pupil across the considered direction, and these phase variations contribute to the signal weighted by the inverse of the distance between the integration point (x', y) and the measured point (x, y). The linear relation between the PWFS signal and the phase tilt cannot be obtained using this formula, but we have demonstrated that the correction orientation for the non-modulation PWFS is right. The AO system can be closed with a successive iteration process[16], and the feasibility of this non-modulation method has been demonstrated[17]. Consequently, this AO system

for the 1.8 m telescope uses the PWFS without any modulation.

In order to analyze the characteristics of the non-modulation PWFS using in the 1.8 m telescope, a closed-loop AO simulation module is established. The simulation parameters are as follows (consistent with the actual 1.8 m telescope):

- Telescope diameter: 1760 mm
- Central obscuration: 280 mm
- Number of actuators of DM: 127
- Number of sub-apertures of PWFS: 13×13
- Working mode of PWFS: non-modulation
- Fried parameter r_0:135 mm

First, the theoretical limit fitting ability of the 127-element DM to the Zernike aberration is analyzed and simulated. The relative error variance (defined as parameter β) is used to describe the correction ability[18]. The parameter β is given by the following expression:

$$\beta = \frac{\mathrm{RMS}_{\_\mathrm{residual}}}{\mathrm{RMS}_{\_\mathrm{initial}}}. \tag{7}$$

In Eq. (7), $\mathrm{RMS}_{\_\mathrm{initial}}$ is the initial RMS error of the wavefront aberration, and $\mathrm{RMS}_{\_\mathrm{residual}}$ is the residual RMS error after correction. The smaller the value is, the smaller the residual wavefront error will be, and the stronger the aberration correction ability. The green histograms in Fig. 3 represent the relative error variance for the top 35 orders of Zernike aberrations, that is to say, the correction ability of the AO system using this 127-element DM is not less than the theoretical fitting ability.

Second, the closed-loop AO simulation module based on the non-modulation PWFS and the 127-element DM is used to correct the top 35 orders of Zernike aberrations, and the blue histograms in Fig. 3 show the correction effect. Due to the limited space sampling of the PWFS with 13×13 sub-apertures, the AO system cannot achieve the theoretical correction ability of the 127-element DM. From the simulation figure, the PWFS correction result is 0.04 larger than that of the theoretical correction for the 28th mode, and the difference is less than 0.015 for the other modes. Consequently, the 127-element AO system using the non-modulation PWFS can be used, as expected, to correct the top 35 orders of Zernike aberrations.

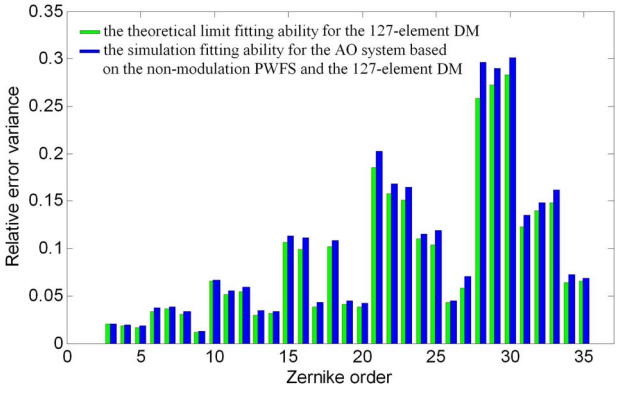

Fig. 3. Relative error variance of the top 35 orders of Zernike aberrations.

Third, the correction ability for the Kolmogorov phase screen composed of 3 to 104 Zernike modes (according to Fried parameter $r_0 = 135$ mm) is also simulated with the 127-element AO system based on the non-modulation PWFS (with 13×13 sampling sub-apertures). The initial and corrected far-field images are shown in Fig. 4, and the correction effect reaches the diffraction-limit level (the Strehl ratio is about 0.97 for the corrected far-field spot). The initial and corrected PWFS detection images are illustrated in Fig. 5; when the closed loop is stabilized, the four sub-pupil images have the same intensity distribution (each of the four sub-pupil images has a 13×13 pixels region).

The full width at half-maximum (FWHM) for the two-dimensional section of the closed-loop spot is illustrated in Fig. 6. If the diffraction-limited FWHM is τ_0, it can be calculated that the x-direction FWHM is $1.02\tau_0$ and the y-direction FWHM is also $1.02\tau_0$.

The above simulation results verify the feasibility of the non-modulation mode for the PWFS and also lay a good theoretical foundation for the development of the field experiment. The detection CCD of the PWFS for the 1.8 m telescope is an OCAM2 camera with a 240×240 pixel-array. Four sub-pupil images of the PWFS are distributed on the CCD, and each corresponds to the 65×65 pixels region (see Fig 7(a)). With the 5×5 pixel-rebin processing, the sampling of each sub-pupil changs to 13×13 pixels (see Fig. 7(b)), which is equivalent to the original AO system based on a Shack–Hartmann wavefront sensor

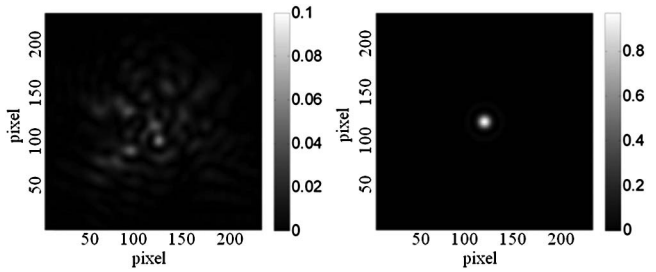

Fig. 4. Simulation results of the initial and corrected far-field images for the turbulence phase screen ($D = 1760$ mm, $r_0 = 135$ mm).

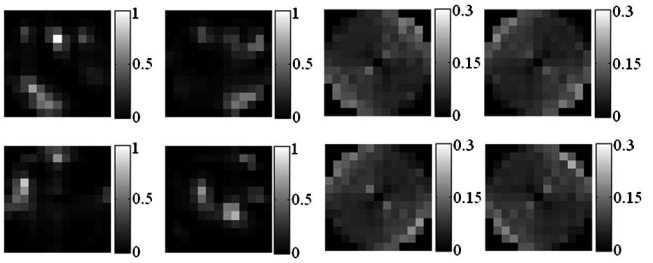

Fig. 5. Simulation results of the initial and corrected PWFS images for the turbulence phase screen ($D = 1760$ mm, $r_0 = 135$ mm).

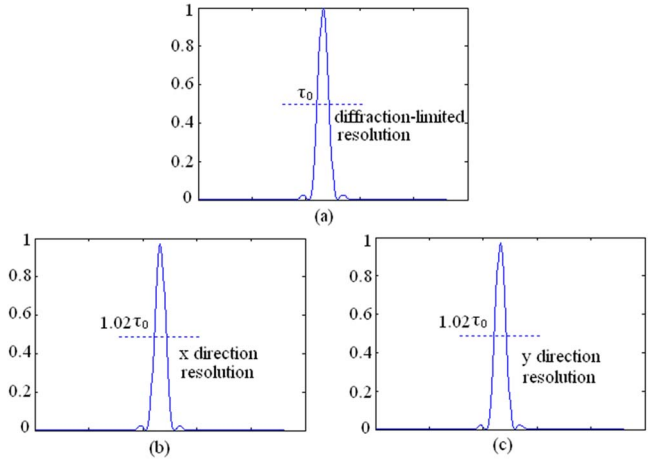

Fig. 6. FWHM of the diffraction-limited spot, and the two-dimensional FWHM of the simulated closed-loop spot.

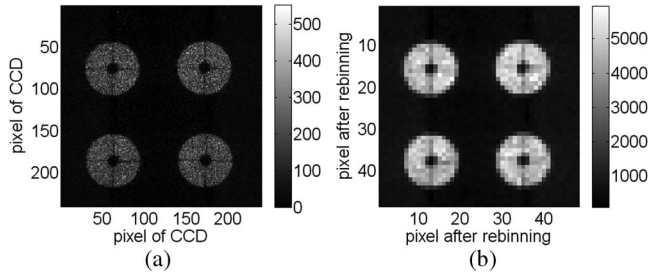

Fig. 7. (a) Original image (each sub-pupil has 65×65 pixels) and (b) rebin image (each sub-pupil has 13×13 pixels).

with 13×13 sampling sub-apertures. Figure 7 is a calibration image that is used to determine the position of the four PWFS sub-pupil images, and the following Fig. 8 illustrates the open-loop and closed-loop images for the actual field experiment.

The optical path length aberrations of a beam are corrected by the mechanical displacement of a DM's surface. There are three main DM families: discrete actuator mirrors using a continuous faceplate; bimorph mirrors, in which the actuator is combined with the faceplate; and segmented mirrors[2]. The DM used in the AO system of the 1.8 m telescope is a 127-discrete actuators mirror, and the arrangement of these 127 actuators in the DM is shown in Fig. 9.

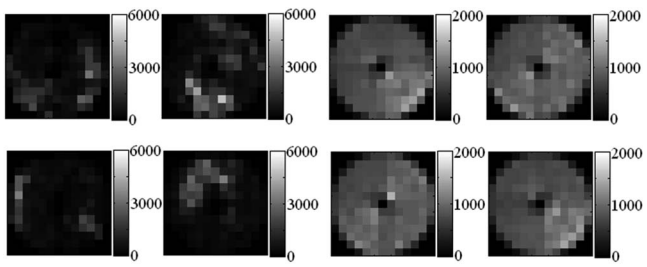

Fig. 8. Open-loop and closed-loop experiment PWFS images.

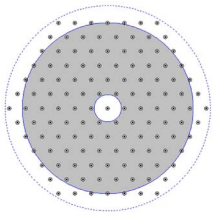

Fig. 9. Space arrangement of the 127 actuators (the outer circle represents the mirror edge of the DM, and the gray area represents 1.8 m telescope pupil plane).

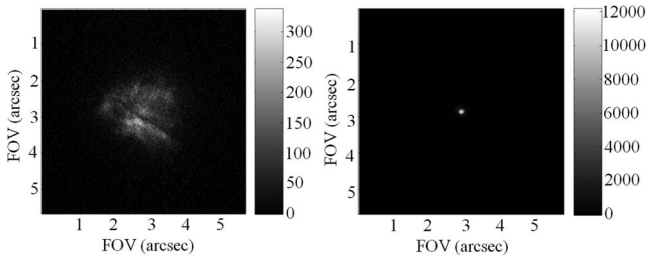

Fig. 10. Open-loop and closed-loop star images (Name: HIP113881, Magnitude: 2.44).

In late October 2014, we performed the final integration, alignment, and calibration of the AO system based on the PWFS, and high-resolution imaging for the first light of the natural stars was obtained. The open-loop and closed-loop star images of the AO system are shown in Fig. 10. The name of this imaging stellar star was HIP113881, and the magnitude of this star was

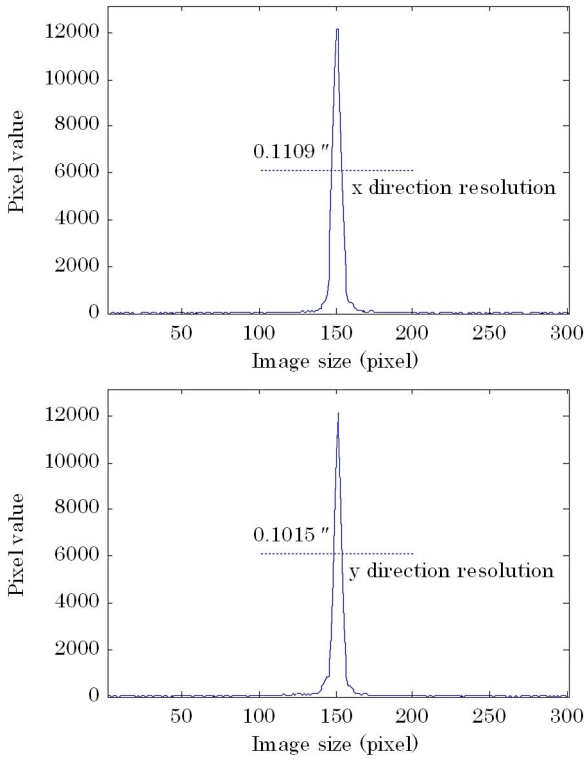

Fig. 11. Two-dimensional section of the closed-loop image.

2.44. The open-loop imaging spot was scattered on the detection surface of the camera due to the atmospheric turbulence, and after closed-loop correction with the AO system, the spot energy was concentrated.

The FWHM of the imaging spot is a criterion method of the actual angular resolution. In order to make a quantitative study on the imaging performance of the AO system, the FWHM for the two-dimensional section of the closed-loop star image is illustrated in Fig. 11. It can be calculated that the x-direction FWHM is $0.1109''$, and the y-direction FWHM is $0.1015''$. The x-direction FWHM is about 1.18 times the diffraction-limited value ($0.1109/0.0938 \approx 1.18$), and the y-direction FWHM is about 1.08 times the diffraction-limited value ($0.1015/0.0938 \approx 1.08$).

Compared with the above simulation results, the x-direction FWHM reaches about 1.16 times the simulation value ($1.18/1.02 \approx 1.16$), and the y-direction FWHM reaches about 1.06 times the simulation value ($1.08/1.02 \approx 1.06$).

In conclusion, the first light of an AO system based on a non-modulation PWFS on a 1.8 m telescope is reported. The results show that the AO system using the non-modulation PWFS can work satisfactorily and the diffraction limit performance can be obtained. A significant advantage of the PWFS is that the number of sub-apertures can be adjusted according to the change of the turbulence, so that the PWFS has better adaptability compared with a Shack–Hartmann wavefront sensor. The corresponding experiment has been carried out and will be reported in the future.

I would like to acknowledge and thank Professor Wenhan Jiang for his guidance and support in the course of this study. This work was supported by the National Natural Science Foundation of China under Grant No. 61008038.

References

1. R. J. Noll, J. Opt. Soc. Am. **66**, 207 (1976).
2. J. W. Hardy, *Adaptive Optics for Astronomical Telescopes* (Oxford University, 1998).
3. W. H. Southwell, J. Opt. Soc. Am. **70**, 998 (1980).
4. L. Yang, L. Hu, D. Li, Z. Cao, Q. Mu, J. Ma, and L. Xuan, Chin. Opt. Lett. **13**, 120801 (2015).
5. R. Ragazzoni, J. Mod. Opt. **43**, 289 (1996).
6. R. Ragazzoni and J. Farinato, Astron Astrophys. **350**, 23 (1999).
7. T. Y. Chew, R. M. Clare, and R. G. Lane, Opt. Commun. **268**, 189 (2006).
8. R. Ragazzoni, A. Ghedina, A. Baruffolo, E. Marchetti, J. Farinato, T. Niero, G. Crimi, and M. Ghigo, Proc. SPIE **4007**, 423 (2000).
9. S. Esposito, A. Riccardi, L. Fini, A. T. Puglisi, E. Pinna, M. Xompero, R. Briguglio, F. Quirós-Pacheco, P. Stefanini, J. C. Guerra, L. Busoni, A. Tozzi, F. Pieralli, G. Agapito, G. Brusa-Zappellini, R. Demers, J. Brynnel, C. Arcidiacono, and P. Salinari, Proc. SPIE **7736**, 773609 (2010).
10. A. H. Bouche, D. S. Acton, R. Biasi, R. Conan, B. Espeland, S. Esposito, J. Filgueira, D. Gallieni, B. A. McLeod, E. Pinna, F. Santoro, G. Trancho, and M. A. Van Dam, Proc. SPIE **9148**, 91480W (2014).
11. F. Quirós-Pacheco, G. Agapito, A. Riccardi, S. Esposito, M. Le Louarn, and E. Marchetti, Proc. SPIE **8447**, 84475L (2012).
12. K. Wei, X. Zhang, H. Xian, W. Ma, A. Zhang, L. Zhou, C. Guan, M. Li, D. Chen, S. Chen, Z. Liao, C. Rao, and Y. Zhang, Chin. Opt. Lett. **8**, 1019 (2010).
13. A. Burvall, E. Daly, S. R. Chamot, and C. Dainty, Opt. Express **14**, 11925 (2006).
14. J. B. Costa, Appl. Opt. **44**, 60 (2005).
15. C. Vérinaud, Opt. Commun. **233**, 27 (2004).
16. S. Wang, C. Rao, H. Xian, J. Zhang, J. Wang, and Z. Liu, Opt. Express **19**, 8135 (2011).
17. S. Wang, C. Rao, A. Zhang, X. Zhang, K. Wei, Y. Tian, Z. Liao, C. Zhang, H. Xian, X. Zhang, and L. Wei, Proc. SPIE **8447**, 84476K (2012).
18. H. Duan, E. Li, H. Wang, Z. Yang, and Y. Zhang, Acta Opt. Sin. **23**, 1143 (2003).